Metall. Res. Technol. **116**, 109 (2019)

https://doi.org/10.1051/metal/2018041

&Metallurgical Research Technology

Available online at:
www.metallurgical-research.org

Regular Article

# Effect of hot rolling on the corrosion behavior of AZ31 magnesium alloy

Abdelkader Hanna[1,2], Achour Dakhouche[3], Kamel Tirsatine[4], Ali Sari[5], Yazid Khereddine[6], Djamel Bradai[4], and Hiba Azzeddine[2,4,*]

[1] Physics and Chemistry of Materials Laboratory, Department of Physics, University Mohamed Boudiaf, 28000 M'sila, Algeria
[2] Department of Physics, University Mohamed Boudiaf, 28000 M'sila, Algeria
[3] Inorganic Materials Laboratory, Department of chemistry, Faculty of Sciences, University of Mohamed Boudiaf, 28000 M'sila, Algeria
[4] Faculty of Physics, USTHB, BP32 El-Alia, Dar El-Beida, Algiers, Algeria
[5] Nuclear Research Center of Birine, Ain-Oussera, Djelfa, Algeria
[6] Centre de Développement des Technologies Avancées, CDTA, Cité du 20 août 1956, Baba-Hassen, 16303 Algiers, Algeria

Received: 12 March 2018 / Accepted: 4 May 2018

**Abstract.** The aim of the present study is to investigate the effect of deformation conditions on the corrosion behavior of AZ31 (Mg-3Al-1Zn, % wt.) in 0.9% NaCl (wt.%) solution. The AZ31 alloy was hot rolled at 360 °C to 20 and 50% of thickness reduction. Electrochemical measurements were used to study the corrosion behavior of AZ31 alloy. Analysis of corrosion products after immersion test was performed using optical microscopy, X-ray diffraction and Raman spectroscopy. The mechanical properties of corroded samples were investigated using tensile test at room temperature. Results indicated that the corrosion rate was strongly affected by the hot rolling level. A lower corrosion potential and reduced polarization resistance was observed after hot rolling compared to the as received AZ31 alloy. The corrosion product was evidenced mainly as $Mg(OH)_2$ compound exhibiting a filiform-like morphology. Apparently, the corrosion improved the room temperature ductility of AZ31 alloy.

**Keywords:** corrosion resistance / magnesium alloy / rolling / deformation / mechanical properties

## 1 Introduction

Magnesium alloys containing Aluminum and Zinc, known as the AZ series magnesium alloys, have been and are widely used in automotive and aerospace industries due to their low density and high specific strength [1,2]. Aluminum, as alloying element improves the sheet formability by modification of the final texture [3], enhances the strength through solid solution effect and develops the corrosion resistance of Magnesium matrix [4]. Usually, Zinc as addition alloying element is used as a grain refiner [5]. Nowadays, AZ series alloys are receiving increasing attention in biomedical engineering as potential biodegradable implant materials for orthopedic applications [6–8]. Wen et al. [9] investigated the corrosion behavior of pure Mg, AZ31, AZ61 and AZ91 alloys in a modified simulated body fluid (m-SBF) using electrochemical testing. They reported that the microstructure and the Al content in the Mg matrix significantly affected the corrosion properties. Moreover, the corrosion resistance of the samples was improved with increasing Al content. On the other hand, high content of Aluminum in Mg based alloy are not advisable due to toxicity issues [10]. Therefore, AZ31 (Mg-3Al-1Zn, % wt.) alloy, a common structural material with low Aluminum content could be a good candidate for biomaterial applications [11]. However, Mg-based alloys generally suffer from poor corrosion resistance and their degradation occurs faster than expected [12]. Atrens and his co-authors [13–17] have provided an extensive review of recent works on the Mg corrosion field and the multiple aspects that determine the corrosion of Mg alloys. According to these authors, the poor corrosion resistance of Mg alloys could be attributed to:

– the internal galvanic corrosion by second phases or impurities elements such Fe, Ni, Cu and Co and;
– the instability of the hydroxide film formed on the Mg matrix surface.

In order to improve the corrosion resistance, several strategies have been proposed such as element alloying [18] and anodic coatings surface treatments [19,20]. However,

* e-mail: azehibou@yahoo.fr

some additives could cause serious concerns for the potential toxic effects [8,18,21]. Furthermore, it was found that thermo-mechanical processing such as extrusion [22], rolling [23–25] or recent severe plastic deformation (SPD) techniques [10,26,27] could be used to improve the mechanical properties and control the corrosion behavior of Mg based alloy, simultaneously. Published data suggest that reducing the grain size to micro or nano-scale may affect the surface roughness parameters, which, in turn, affect the degradation of Mg based alloys [10,26]. Ren et al. [28] reported that the corrosion rate of as-forged high-purity Mg increased after heat treatment at 500 °C for 10 h, due to grain growth and coarsening. Indeed, the improved corrosion resistance was explained by the uniform distribution, the decrease of the volume fraction of second phase and the relieving of the internal stress [29]. The crystallographic orientations of the grains were thought as another parameter that strongly influences the corrosion anisotropy [30,31]. For example, the surface of hot rolled AZ31 sample, with dominant (0001) basal planes, was found more corrosion resistant than the cross-section surface, which mainly consisted of $\{10\bar{1}0\}$ and $\{11\bar{2}0\}$ prismatic crystallographic planes [30]. It is well known that deformation conditions like processing type, temperature and strain rate could significantly affect the mechanical properties of the metals and alloys. Nevertheless, the relationship between deformation conditions and corrosion behavior in Mg based alloys is not well established yet. Thereby, the aim of the present work is to investigate the effect of hot rolling at 360 °C on the microstructural evolution and corrosion behavior of a commercial AZ31 alloy.

## 2 Experimental procedure

### 2.1 Materials and plastic deformation conditions

The AZ31 sheets with 2.2 mm of thickness were kindly supplied by MagIC – Magnesium Innovations Center, Germany, with the chemical composition shown in Table 1. The rolling experiments were conducted at a nominal rolling temperature of 360 °C. The total reductions in thickness were 20 and 50 with 10% reduction per pass.

### 2.2 Optical microscopic observation

Microstructural examination was performed in the rolling plane at mid-thickness of the rolled sheets by optical microscopy. Surface preparation consisted of grinding with progressively finer SiC paper followed by mechanical polishing using diamond solution with particle sizes ranging between 3 and 1 μm. The grain structure revealing was achieved by subsequent etching in a solution of acetic picral.

### 2.3 Vickers microhardenss measurement

Vickers microhardness (Hv) measurements were taken with a load of 2 N maintained for a dwell time of 10 s using a SHIMADZU type HMV-2 tester. At least five indentations were used to obtain the average hardness values.

**Table 1.** Chemical composition of AZ31 alloy.

| Al | Zn | Mn | Ca | Cu | Fe | Mg |
|---|---|---|---|---|---|---|
| 3.45 | 0.98 | 0.28 | 0.002 | 0.002 | 0.004 | Balance |

### 2.4 Tensile test

Tensile tests were carried out using Zwick Roell tester at room temperature to failure with strain rate of $10^{-4}\,s^{-1}$. Flat specimens with gauge dimensions of 6 mm × 12 mm were machined from the rolling plane of the samples.

### 2.5 X-ray diffraction measurement

X-ray diffraction (XRD) patterns were recorded using X'PERT PRO MPD diffractometer operating at 40 kV and 40 mA, using Cu-Kα radiation and fitted with the X'Celerator detector. The data were collected over a range of 20–120° in 2θ with a step size of 0.026° and scan speed of 0.18°/sec, using the scanning X'Celerator detector.

### 2.6 Raman spectroscopy

The Raman spectra of corroded samples were obtained using Horiba LabRAM HR Evolution Spectrometer. The laser power was 17 mW, using the 633 nm line of a He-Ne laser. The spectra were recorded over the range of 100 to 4000 $cm^{-1}$.

### 2.7 Electrochemical measurements

Electrochemical tests were conducted using an AUTOLAB PGSTAT302N electrochemical work station and a standard three-electrode cell, where the sample is the working electrode, a platinum plate as the counter electrode, and a calomel electrode (SCE)(0.24vs.SHE) as the reference electrode. The samples were embedded in an epoxy resin to isolate a 1 $cm^2$ area from the non-studied surfaces, and were then immersed in a 0.9% NaCl (wt. %) solution at ambient temperature. The open-circuit potential (OCP) was measured for at least 60 minutes for all samples. The polarization curves were recorded in the range of −2.6 to 0 V vs. SCE with scan rate 2 $mV.s^{-1}$. The impedance measurements were performed after the open circuit potential with a sinusoidal potential signal with amplitude of 10 mV in the frequency range from $10^{-2}$ Hz to $10^5$ Hz. Experimental curves were fitted using the Zview software.

## 3 Results and discussion

Figure 1 illustrates the microstructure of the as received AZ31 alloy and after hot rolling to 20 and 50% thickness reduction. The mean grain size of AZ31 alloy is presented in Table 2. The microstructure of the as received AZ31 alloy is typical of equiaxed granular with an average size about 18 μm. The rolling microstructure revealed equiaxed grains with the presence of significant amounts of lenticular twins after 20% of thickness of reduction (see arrows in

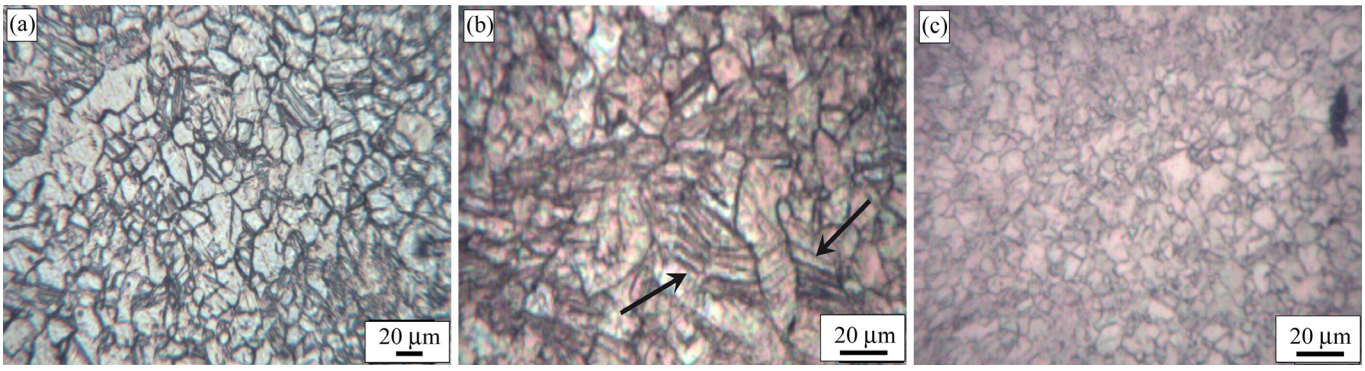


**Fig. 1.** Optical micrograph of AZ31 alloy: a) as received, b) hot rolled of 20% of thickness reduction and c) hot rolled to 50% of thickness reduction.

**Table 2.** Mean gain size ($d$) and microhardness ($Hv$) values of the as received and hot rolled AZ31 alloy.

| | As received | 20% | 50% |
|---|---|---|---|
| $d$ (µm) | 18.0 | 10.8 | 8.2 |
| $Hv$ | 69.3 | 80.2 | 75.6 |

Figure 1b). The microstructure of AZ31 after hot rolling to 50% thickness reduction exhibits a bimodal microstructure in which small grains appeared after dynamic recrystallization process. Quiet similar microstructure was reported by Abdessameud et al. [32] in dynamically recrystallized AZ31 alloy after hot rolling at 450 °C to 20% thickness reduction. As shown in Table 2, the grain size decreased from 18 to 8 µm after 50% of thickness of reduction. Table 2 lists the evolution of Vickers microhardness of as received AZ31 and after hot rolling to 20 and 50% of thickness reduction. The microhardness increases from 69 Hv in the as received state to 80 Hv after 20% of thickness reduction. The improvement of the hardness could be attributed to the strain hardening effect and grain refinement. However, the microhardness seems to decrease (75 Hv) after hot rolling to 50% of thickness reduction. This decrease could be attributed to the complex competitive mechanisms of generation and annihilation of dislocation by recovery phenomenon and dynamic recrystallization as corroborated by microstructure evolution as shown in Figure 1c.

Figure 2a presents the open circuit potential (OCP) plots of the as received and hot rolled to 20 and 50% of thickness reduction AZ31 alloy in 0.9% NaCl solution. It can be noticed that the three samples exhibit the same OCP evolution which increases rapidly and reaches a steady state at −1.55 V after about 360 sec of immersion. The steady state condition indicates that dynamic balance has been established between the anodic and catholic reactions (development of the corrosion activity and the deposit of the corrosion products on the surface of the alloy) [33]. Some researchers reported that of OCP plot exhibits fluctuation during the measurement in Mg based alloys immersed in NaCl solution [22,34–37]. It was suggested such fluctuations resulted from the fact that no equilibrium has been achieved at the electrode/solution interface [34] and that no dense and effective anticorrosion film was created on the surface [38,39].

The polarizations curves of as received and hot rolled to 20 and 50% of thickness reduction AZ31 alloy in 0.9% NaCl solution are shown in Figure 2b. Resulting electrochemical parameters from the fitting and the correlated corrosion rates are listed in Table 3. The corrosion potential, ($E_{corr}$) and the corrosion current density ($I_{corr}$) values were determined by extrapolating the linear Tafel segments of the anode and cathode polarization curves. As shown in Figure 2b, the polarization curves for three samples exhibit very similar trends where the anodic and cathodic branches are not symmetrical. This similarity translates the identical hydrogen evolution in the cathodic polarization curve and the formation of $Mg^{2+}$ due to the dissolution of Mg in the anodic polarization curve [40,41].

It can be observed from Table 3 that the polarization resistance ($R_p$) decreases with increasing reduction of thickness and the corrosion current density ($I_{corr}$) increases with increasing deformation strain. According to the Stern-Geary equation, a better corrosion resistance is obtained when $I_{corr}$ is lower, following the equation [42]:

$$R_p = \frac{\beta_a \beta_c}{2.303(\beta_a + \beta_c) I_{corr}}, \quad (1)$$

where $\beta_a$ and $\beta_c$ are the anodic and cathodic slopes, respectively.

As can be noticed in Table 3, the corrosion potential $E_{corr}$ of AZ31 alloy is shifted towards negative value with increasing deformation level. So, the as received AZ31 is nobler than hot rolled samples. Similarly, the corrosion rate of hot rolled AZ31 alloy increases more from 0.19 mm/year for the as received AZ31 alloy to 2.34 mm/year after 50% of thickness reduction. However, it has been stated that corrosion rate values estimated from Tafel extrapolation are not often in good agreement with those measured by weight loss or hydrogen evolution [17,43]. In fact, the value of the corrosion rate from the polarization curves may be orders of magnitude too small [17,43]. However, it is worth noting that these values fall within tabulated data range for AZ series (see Table 2 in [14]). Atrens et al. [16] have pointed out the importance of impurity elements such as Fe, Ni, Cu, Co that are harmful to pure Mg and Mg alloys. These authors stated that high corrosion rates may occur for Mg containing any of these elements at a concentration above their tolerance limit. Among these elements, Fe

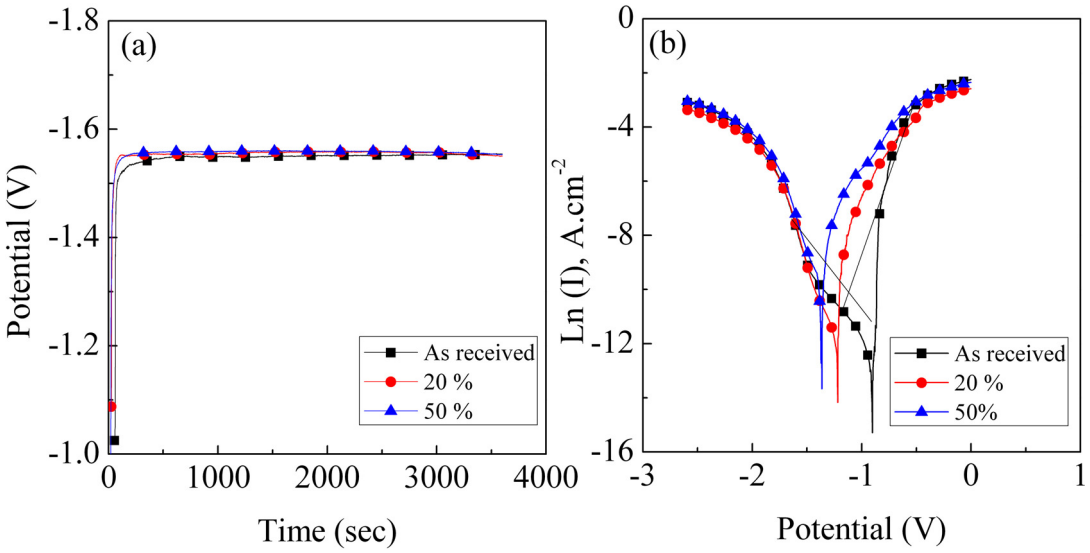


**Fig. 2.** a) Open circuit potentiel (OCP), b) Potentiodynamic polarisation curves of as received AZ31 alloy and hot rolled to 20 and 50% of thickness reduction in 0.9% NaCl solution.

**Table 3.** Electrochemical parameters obtained from the potentiodynamic polarization test.

| | $E_{corr}$ (Volt) | $I_{corr}$ ($\mu$A.cm$^{-2}$) | $R_p$ ($\Omega$.cm$^2$) | Corr. rate (mm/year) |
|---|---|---|---|---|
| As received | −0.88 | 4.20 | 2603.4 | 0.19 |
| 20% | −1.21 | 5.46 | 1055.4 | 0.28 |
| 50% | −1.36 | 49.30 | 398.1 | 2.34 |

content is determinant. Its tolerance limit is ~ 180 ppm Fe) [16]. From Table 1, it is obvious that the Fe content is far above the tolerance limit and hence may lead to galvanic acceleration of the corrosion of the alpha-Mg matrix by the Fe-rich BCC phase. Moreover, the corrosion rate of immersed alloys depends strongly on the duration of immersion test. For example, Wen et al. [9] have established a hierarchy of the corrosion rates of four alloy samples in m-SBF as follows AZ91D < AZ61 < AZ31 < pure Mg after immersion for 1 day. This order changed to AZ91D < pure Mg < AZ61 < AZ31 after immersion for 24 days [9].

The present results indicate that the as-received AZ31 alloy has better corrosion resistance than deformed ones. Similar result has been reported [44–47] which demonstrated that deformation and grain refinement do not improve the corrosion resistance of Mg based alloy. However, Silva et al. [47] have shown that deformation processing could change the corrosion behavior. Especially, High pressure torsion (HPT) processing led to general corrosion compared to localized corrosion in the as cast and hot rolled pure Mg [47]. Saikrishna et al. [46] reported that the decrease in the corosion resistance of the deformed Mg based alloy could be attributed to the texture effect and large variations in grain size which resulted in non-uniform galvanic intensities. This suggestion fit well with the microstructures found in the present work. Unifomity of grain size distibution can obviously be noticed in the microstructure of as received AZ31 alloy as shown in Figure 1a. While a bimodal grain size distribution with a high fraction of twins can be noticed in hot rolled alloy samples (Figs. 1b-c). Ralston et al. [48] reported that the effect of grain refinement on the corrosion resistant depends on the corrosion current values. When the corrosion current was higher than $10^{-5}$ A.cm$^2$, the grain refinement can lead to a substantial corrosion rate of the material. While, if the corrosion current was lower than $10^{-5}$ A.cm$^2$, the grain boundaries could help to develop a passive layer in the materials surface. This suggests that grain refinement may improve the corrosion resistance [48].

Figure 3 shows the Nyquist plots following 1h OCP immersion in 0.9% NaCl solution of as received AZ31 alloy and hot rolled to 20 and 50% of thickness reduction. All three samples display one large capacitive loop at high frequency extending to an inductive loop characterized by data in the second quadrant in the region of low frequencies. Such analogy means that the as received and as rolled AZ31 alloys have similar corrosion mechanisms but different rates. Usually, the area of high frequency is used to detect the surface defects, whereas the medium and low frequency detect the processes within the corrosion product at the metal/corrosion product interface, respectively [49]. Furthermore, the presence of inductance loop is characteristic of Mg based alloy and is widely observed in Nyquist plots in various immersion solutions [9,11,18,36,37,40,50,51]. The inductance loop suggests the occurrence of pitting corrosion, dissolution of the protective film and sample surface destruction [50]. On

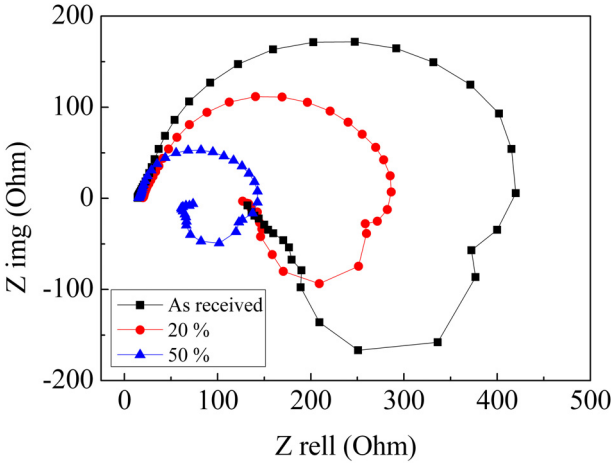


**Fig. 3.** Nyquist plots in NaCl solution of as received AZ31 alloy and hot rolled to 20 and 50% of thickness reduction.

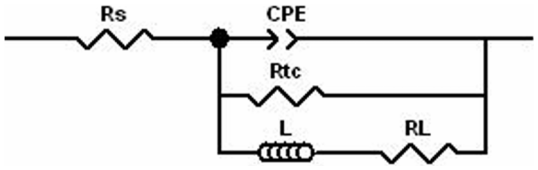


**Fig. 4.** Equivalent circuit for as received AZ31 alloy and hot rolled to 20 and 50% of thickness reduction in 0.9% NaCl solution.

the other hand, it was ascribed to the existence of metastable $Mg^{+}$ during the dissolution of Mg alloy [11] or to the relaxation of surface adsorbed species like $Mg(OH)^{+}$ and $Mg(OH)_2$ [48].

It is obvious from Figure 3 that the impedance values decrease with increasing deformation strain. Moreover, the diameter of capacitive loop, which represents the polarization resistance of the sample, in as received AZ31 alloy was larger than that of as rolled sample, implying that the as received AZ31 alloy has higher corrosion resistance. This finding confirms the result obtained from polarization curves.

In order to analyze the corrosion mechanisms of the present AZ31 alloys, the corresponding equivalent circuit and the fitting data of the EIS curves are presented in Figure 4 and Table 4, respectively.

In the equivalent circuit, $R_s$ is a solution resistance of bulk electrolyte between reference and working electrodes. Actually, the $R_s$ values depend on the conductivity of testing medium and the geometry of employed cell and do not contribute in the electrode process [35]. *CPE* is a constant phase element that represents the capacitance in the high frequency area of the corrosion products formed on the alloy surface. The *CPE* is defined by two values, $Y$ and $n$. If $n = 1$, *CPE* will be identical to a capacitor and if $n = 0$, *CPE* represents a resistance. It is to be noted that the CPE is generally employed instead of the capacitance in case of the non-homogeneity of the sample surface [52]. $R_{tc}$ is the charge transfer resistance of the corrosion process. $L$ and $R_L$ are inductance and inductance resistance of the inductance loop in low frequency, respectively.

Data from Table 4 shows that the $R_2$ value of as received AZ31 alloy (453.8 $\Omega.cm^{-2}$) is higher than those of the as rolled AZ31 alloy for 20% (280.9 $\Omega.cm^{-2}$) and 50% of thickness reduction (133.8 $\Omega.cm^{-2}$). This result confirms that the oxidation film formed at the surface of as received AZ31 alloy has better capacity to protect the alloy against corrosion. The diameter of the inductive loop depends on the size and intensity of the localized corrosion in the sample surface [53]. It was observed that the small corrosion pits resulted in a strong induction loop, and more the corrosion was severely localized, more the induction loop became less pronounced [53].

Figure 5 illustrates the XRD patterns of as received AZ31 alloy and hot rolled to 50% thickness reduction after 3 h immersion in 0.9% NaCl solution, respectively. It can be observed that the as received AZ31 alloy presents only the Mg matrix peaks (Fig. 5a). Small peaks appeared around $2\theta = 18.6$, 37.7 and 68.7° in both samples after 3 h of immersion in 0.9% NaCl solution and were assigned to the magnesium hydroxide $Mg(OH)_2$ compound (Figs. 5b and c). Saikrishna et al. [46] found that the amount of $Mg(OH)_2$ on AZ31 samples processed by friction stir processing (FSP) was more profuse comparatively to the unprocessed AZ31 sample. It is well known that the corrosion reaction of Mg based alloys lead to the formation $Mg(OH)_2$ accompanied by hydrogen evolution, following the equations [13]:

Anodic reaction:

$$M_g \rightarrow Mg^2 + 2e^-, \quad (2)$$

Cathodic reaction:

$$H_2O + 2e^- \rightarrow 2OH^- + H_2, \quad (3)$$

The total reaction:

$$M_g + H_2O \rightarrow M_g(OH)_2 + H_2, \quad (4)$$

However, it has been reported that the corrosion product film on the Mg surface is multilayered and consisted of a thin inner MgO layer covered with $Mg(OH)_2$ [54–57]. Upon hydration, the MgO oxide forms soluble species and could gradually transform to $Mg(OH)_2$ [55,57]. Moreover, the thickness of MgO oxide layer was found to decrease with increasing Al content in Mg-Al alloys [58].

For more details on the corrosion product, a Raman spectrum was acquired from the as received and hot rolled to 50% thickness reduction AZ31 samples corroded in potentiodynamic measurement in 0.9% NaCl solution as shown in Figure 6. Two disguised peaks can be noticed in both samples around 440.5 and 3650.26 $cm^{-1}$. A third one with a weak intensity can be observed around 1643.9 $cm^{-1}$. According to the literature [59] the peaks around 440.5 and 3650.26 $cm^{-1}$ could be attributed to the $Mg(OH)_2$. Frankly, the peak observed at 1643.9 $cm^{-1}$ could not be assigned to any possible corrosion products in Mg based alloy such as $Mg(OH)_2$, MgO or $MgCl_2$ [60].

In order to evidence the corrosion morphology, optical micrographics have been taken from the surface of as received and hot rolled AZ31 alloy after 3 h of immersion in

**Table 4.** Electrochemical parameters obtained from the fits of the experimental EIS data.

| | $R_s$ ($\Omega.cm^{-2}$) | *CPE* ($F.cm^{-2}$) | | $R_{tc}$ ($\Omega.cm^{-2}$) | L ($H.cm^{-2}$) | $R_L$ ($\Omega.cm^{-2}$) |
|---|---|---|---|---|---|---|
| | | *Yn* | | | | |
| As received | 14.5 | $8.0\,10^{-5}$ | 0.813 | 453.8 | 179.4 | 186.6 |
| 20% | 20.1 | $7.110^{-5}$ | 0.825 | 280.9 | 197.2 | 192.6 |
| 50% | 15.4 | $1.3\,10^{-4}$ | 0.866 | 133.8 | 69.25 | 70.57 |

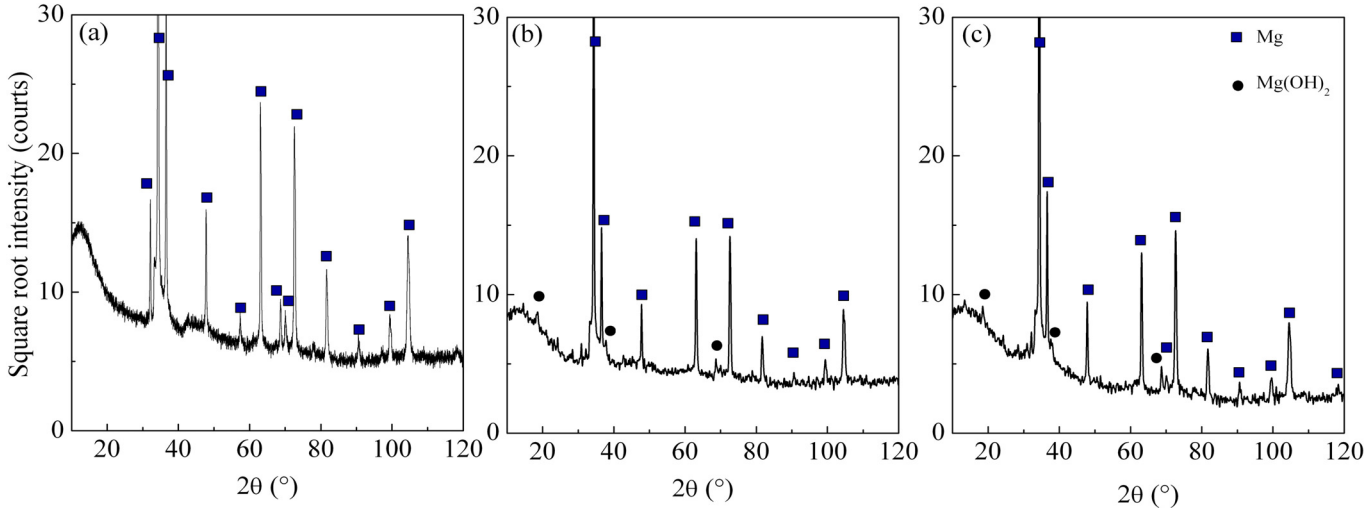


**Fig. 5.** XRD patterns of: a) as received AZ31 alloy and after 3 h of immersion in 0.9% NaCl solution, b) as received AZ31 alloy and c) hot rolled to 50% thickness reduction.

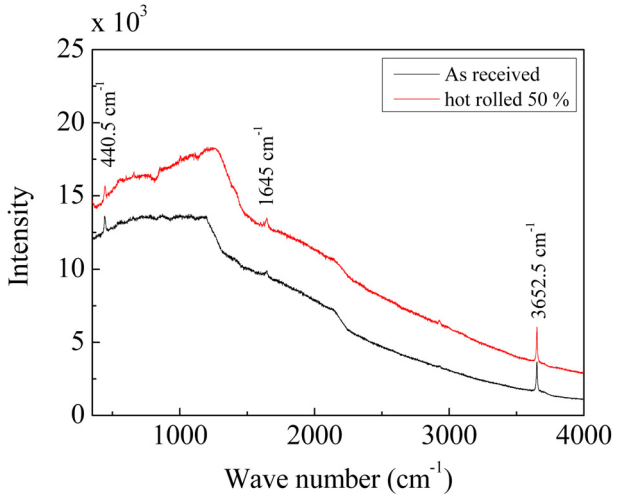


**Fig. 6.** Raman spectra of as received and hot rolled to 50% thickness reduction AZ31 samples after electrochemical measurement.

0.9% NaCl, they are illustrated in Figure 7. As already observed by Atrens et al. [17], the corroded areas are typically dark, attributed to increased surface roughness that no longer provides a shiny reflective metallic appearance. The macrographs of all samples show that the corrosion started from the edges of the samples and was inhomogeneous. The corrosion of all AZ31 samples reveals a typical "filiform-like" morphology that propagates all over the alloy surface with increasing deformation strain. Furthermore, it can be noticed that the pitting corrosion increases with increasing deformation strain (thickness reduction). Similar filiform-like corrosion morphology has been reported in many Mg based alloys [36,53,61]. Such filiform-like corrosion morphology is associated with the reported scenario whereby local anode and cathode sites dynamically evolve [36,62,63]. Moreover, it was reported that initiation and propagation of the filiform corrosion are related to crystallography texture of the sample, and their propagation is influenced by changes in orientation at grain and twin boundaries [53,64]. The correlation of the propagation and morphology of the corrosion products with microstructure and texture of the alloy samples is an ongoing research activity of the present authors. Figure 8 shows the true stress-strain curves of as received and hot rolled AZ31 alloy and after 3 h of immersion in 0.9% NaCl solution. The mechanical properties extracted from the plots of all samples are listed in Table 5.

As can be noticed before the immersion test the tensile, yield strength (TYS) and ultimate tensile strength (UTS) of AZ31 alloy increase with increasing thickness of reduction. In contrast, the elongation to failure decreases from 14.4% to 10.6% after 50% of thickness reduction. Such values are in good agreement with those already reported in pure Mg and Mg based alloys [65].

The immersion test for 3 h in 0.9% NaCl results in a big a drop in TYS and UTS for the three AZ31 samples. However, Reddy et al. [66] reported that the TYS of friction stir welding

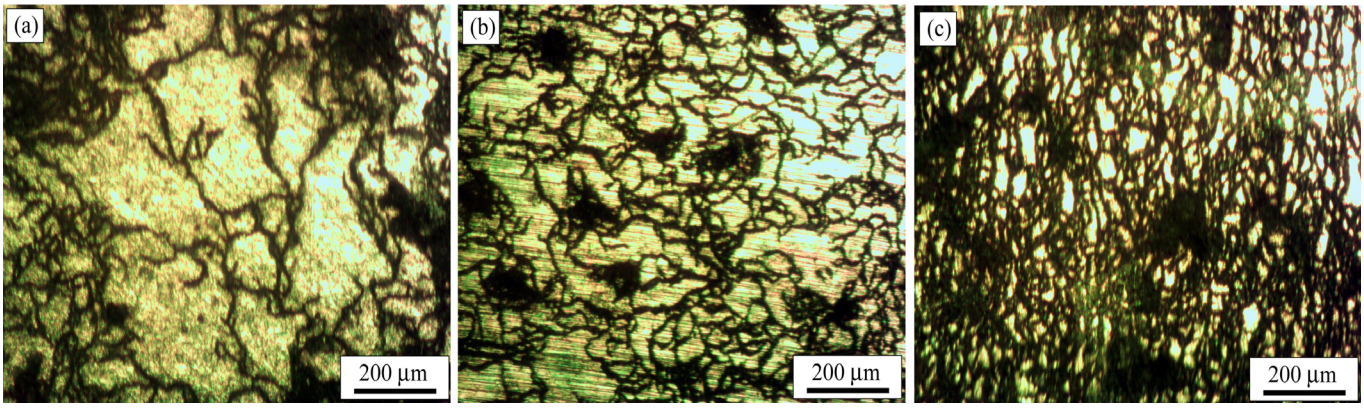


**Fig. 7.** Optical micrographs of a) as received and hot rolled for b) 20%, c) 50% thickness reduction AZ31 alloy after 3 h of immersion in 0.9% NaCl solution.

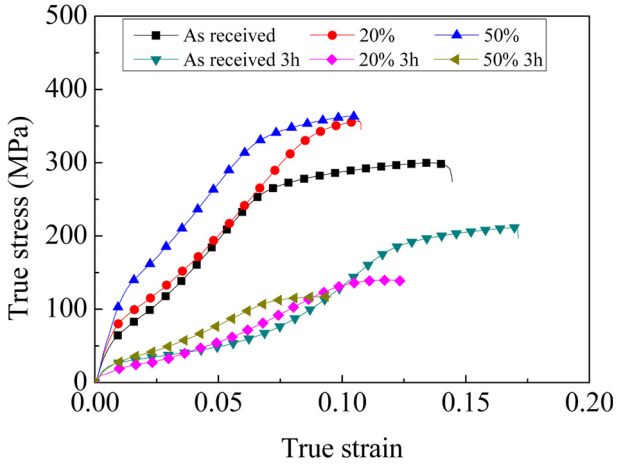


**Fig. 8.** True stess-true strain curves of AZ31 alloy before and after 3 h of immersion in 0.9% NaCl solution.

**Table 5.** Mechanical properties of AZ31 alloys obtained from tensile test: tensile yield strength (TYS), ultimate tensile strength (UTS) and elongation to failure (El).

| Sample | TYS (MPa) | UTS (MPa) | El (%) |
|---|---|---|---|
| As received | 94.2 | 299.6 | 14.4 |
| Hot rolled 20% | 112.7 | 355.4 | 10.7 |
| Hot rolled 50% | 161.1 | 363.2 | 10.6 |
| As received corroded 3 h | 32.9 | 211.5 | 17.1 |
| Hot rolled 20% corroded 3 h | 26.3 | 139.6 | 12.3 |
| Hot rolled 50% corroded 3 h | 39.1 | 116.3 | 9.5 |

(FSW) AZ31 alloy after corrosion in 3.5% NaCl for 24 h was slightly higher than the FSW deformed AZ31 alloy. Table 5 consigns quite interesting results where the elongation to failure increases in corroded samples compared to the non-corroded one. Except, for rolled to 50% thickness reduction samples were very close (10.6 before immersion test vs. 9.5% after immersion test). Apparently, the corrosion of AZ31 alloy improves the room temperature ductility compared to the non corroded samples.

The present findings are in line with many works that have demonstrated the pertinence of performing tensile test on Mg-based alloys as biomaterials, in order to correlate the mechanical properties with the corrosion features mainly degradation rate [66–68].

## 4 Conclusion

From the results of the present investigation, following conclusions have been drawn:

- grain refinement down to 8 µm of the AZ31 alloy led to lower resistance corrosion in 0.9%NaCl solution;
- the corrosion rate of AZ31 alloy increases with the increase of thickness reduction by hot rolling;
- the distribution of grain size and uniform microstructure are key factors of corrosion improvement resistance of the alloys;
- XRD and Raman spectra confirm the formation of Mg $(OH)_2$ film with filiform-like structure on surface of the immersed sample in 0.9% NaCl solution;
- tensile test before immersion revealed that the TYS and UTS of AZ31 alloy increase with increasing thickness of reduction. However, the immersion test in 0.9% NaCl for 3 h conducts to a big drop in the mechanical properties for three AZ31 samples. However, the elongation to failure was higher in corroded samples than non-one. Obviously, corrosion improves the room temperature ductility of AZ31 alloy after immersion tests in 0.9% NaCl solution.

The authors are deeply grateful to Dr-Ing. Norbert Hort and Dr. DietmarLetzig from MagIC – Magnesium Innovations Center, Germany, for kindly providing the AZ31 alloy. Thank you to Prof. N. Bouaouadja from Sétif 1 University, Algeria, for the help and assistance during tensile tests.

## References

1. J.T. Carter, R. Verma, P.E. Krajewski. Mechanical behavior of AZ31 sheet materials at room and elevated temperature magnesium technology 2008, in: JT Mihriban O. Pekguleryuz et al. (Eds.), Warrendale, PA: TMS 2008, pp. 69–74.
2. P.E. Krajewski, S. Kim, J.T. Carter, R. Verma, Magnesium sheet: automotive applications and future opportunities, Trends Met. Mater. Eng. **20**, 60–68 (2007)

3. X. Huang, K. Suzuki, Y. Chino, M. Mabuchi, Influence of aluminum content on the texture and sheet formability of AM series magnesium alloys, Mater. Sci. Eng. A **633**, 144–153 (2015)
4. J. Hirsch, T. Al-Samman, Superior light metals by texture engineering: optimized aluminum and magnesium alloys for automotive applications, Acta. Mater. **61**, 818–843 (2013)
5. M. Esmaily, J.E. Svensson, S. Fajardo, N. Birbilis, G.S. Frankel, S. Virtanen, R. Arrabal, S. Thomas, L.G. Johansson, Fundamentals and advances in magnesium alloy corrosion, Prog. Mater. Sci. **89**, 92–193 (2017)
6. F. Witte, V. Kaese, H. Switzer H, A.M. Lindenberg, C.J. Wirth, H. Windhag, In vivo corrosion of four magnesium alloys and the associated bone response, Biomaterials **20**, 3557–3563 (2005)
7. F. Witte, N. Hort, C. Vogt, S. Cohen, K.U. Kainer, R. Willumeit, F. Feyerabend, Degradable biomaterials based on magnesium corrosion, Curr. Opin. Solid State Mater. Sci. **12**, 63–72 (2008)
8. X.B. Chen, D.R. Nisbet, R.W. Li, P.N. Smith, T.B. Abbott, M.A. Easton, D.H. Zhang, N. Birbilis, Controlling initial biodegradation of magnesium by a biocompatible strontium phosphate conversion coating, Acta. Biomater. **10**, 1463–1474 (2014)
9. Z. Wen, C. Wu, C. Dai, F. Yang, Corrosion behaviors of Mg and its alloys with different Al contents in a modified simulated body fluid, J. Alloys Compd. **488**, 392–399 (2009)
10. B.R. Sunil, A.A. Kumar, T.S.S. Kumar, U. Chakkingal, Role of biomineralization on the degradation of fine grained AZ31 magnesium alloy processed by groove pressing, Mater. Sci. Eng. C **33**, 1607–1615 (2013)
11. Y. Song, D. Shan, R. Chen, F. Zhang, E.H. Han, Biodegradable behaviors of AZ31 magnesium alloy in simulated body fluid, Mater. Sci. Eng. C **29**, 1039–1045 (2009)
12. N.T. Kirkland, N. Birbilis, Magnesium biomaterials design, testing, and best practice, Springer International Publishing, New York, 2014.
13. G.L. Song, A. Atrens, Corrosion mechanisms of magnesium alloys, Adv. Eng. Mater. **1**, 11–33 (1999)
14. M. Liu, P.J. Uggowitzer, A.V. Nagasekhar, P. Schmutz, M. Easton, G. Song, A. Atrens, Calculated phase diagrams and the corrosion of die-cast Mg–Al alloys, Corrosion Sci. **51**, 602–619 (2009)
15. A. Atrens, M. Liu, N.I. ZainalAbidin, Corrosion mechanism applicable to biodegradable magnesium implants, Mater. Sci. Eng. B **176**, 1609–1636 (2011)
16. A. Atrens, G.L. Song, F. Cao, Z. Shi, P.K. Bowen, Advances in Mg corrosion and research suggestions, J. Magnes. Alloy. **1**, 177–200 (2013)
17. A. Atrens, G.L. Song, M. Liu, Z. Shi, F. Cao, M.S. Dargusch, Review of recent developments in the field of magnesium corrosion, Adv. Eng. Mater. **17**, 400–453 (2015)
18. M.B. Kannan, R.K.S. Raman, In vitro degradation and mechanical integrity of calcium-containing magnesium alloys in modified-simulated body fluid, Biomaterials **29**, 2306–2314 (2008)
19. D. Zhang, Y. Gou, Y. Liu, X. Guo, A composite anodizing coating containing superfine Al2O3 particles on AZ31 magnesium alloy, Surf. Coat. Technol. **236**, 52–57 (2013)
20. S. Jafari, R.K. Singh Raman, In-vitro biodegradation and corrosion-assisted cracking of a coated magnesium alloy in modified-simulated body fluid, Mater. Sci. Eng. C **78**, 278–287 (2017)
21. Y. Nakamura, Y. Tsumura, Y. Tonogai, T. Shibata, Y. Ito, Differences in behavior among the chlorides of seven rare earth elements administered intravenously to rats, Fund. Appl. Toxicol. Sci. **37**, 106–116 (1997)
22. H. Xu, X. Zhan, G.K. Zhang, Y. Shi, J. Ren, Effect of extrusion on corrosion behavior and corrosion mechanism of Mg-Y alloy, J. Rare Earths **34**, 315–327 (2016)
23. H. Wang, Y. Estrin, H. Fu, G.L. Song, Z. Zúberová, The effect of pre-processing and grain structure on the bio-Corrosion and Fatigue Resistance of Magnesium Alloy AZ31, Adv. Eng. Mater. **9**, 967–972 (2007)
24. X.N. Gu, X.H. Xie, N. Li, Y.F. Zheng, L. Qin, In vitro and in vivo studies on an Mg–Sr binary alloy system developed as a new kind of biodegradable metal, Acta. Biomater. **8**, 2360–2374 (2012)
25. Wei-li Cheng, Shi-chao Ma, Yang Bai, Ze-qin Cui, Hong-xia Wang, Corrosion behavior of Mg-6Bi-2Sn alloy in the simulated body fluid solution: the influence of microstructural characteristics, J. Alloy. Compd. **731**, 945–954 (2018)
26. B.R. Sunil, T.S.S. Kumar, U. Chakkingal, V. Nandakumar, M. Doble, V. Devi Prasad, M. Raghunath, In vitro and in vivo studies of biodegradable fine grained AZ31 magnesium alloy produced by equal channel angular pressing, Mater. Sci. Eng. C **59**, 356–367 (2016)
27. J.H. Gao, S.K. Guan, Z.W. Ren, Y.F. Sun, S.J. Zhu, B. Wang, Homogeneous corrosion of high pressure torsion treated Mg–Zn–Ca alloy in simulated body fluid, Mater. Lett. **65**, 691–693 (2011)
28. Y.B. Ren, J.J. Huang, K. Yang, B.C. Zhang, Z.M. Yao, H. Wang, Study of bio-corrosion of pure magnesium, Acta. Metall. Sin. **41**, 1228–1232 (2005) (in Chinese)
29. Xue-Nan Gu, Shuang-Shuang Li, Xiao-Ming Li, Yu-Bo Fan, Magnesium based degradable biomaterials: a review, Front. Mater. Sci. **8**, 200–218 (2014)
30. G.L. Song, The effect of texture on the corrosion behavior of AZ31 Mg alloy, JOM **64**, 671–679 (2012)
31. G.L. Song, R. Mishra, Z.Q. Xu, Crystallographic orientation and electrochemical activity of AZ31 Mg alloy, Electrochem. Commun. **12**, 1009–1012 (2010)
32. S. Abdessameud, D. Bradai, Microstructure and texture evolution in hot rolled and annealed magnesium alloy TRC AZ31, Can. Metall. Q. **48**, 433–442 (2009)
33. N. Zidane, Y. Ait Albrimi, A. Ait Addi, R. Ait Akbour, J. Douch, A. Nahlé, M. Hamdani, Effect of gadolinium content on the corrosion behavior of magnesium alloys in 1 wt.%NaCl solution, Portugaliae Electrochimica Acta. **33**, 289–304 (2015)
34. Y. Xin, T. Hu, P.K. Chu, Influence of test solutions on in vitro studies of biomedical magnesium alloys, J. Electrochem. Soc. **157**, C238–C243 (2010)
35. Y.J. Zhang, C.W. Yan, F.H. Wang, W.F. Li, Electrochemical behavior of anodized Mg alloy AZ91D in chloride containing aqueous solution, Corros. Sci. **47**, 2816–2831 (2005)
36. C.Q. Li, D.K. Xu, X.B. Chen, B.J. Wang, R.Z. Wu, E.H. Han, N. Birbilis, Composition and microstructure dependent corrosion behaviour of Mg-Li alloys, Electrochim. Acta. **260**, 55–64 (2018)
37. J. Yang, J. Peng, E.A. Nyberg, F.S. Pan, Effect of Ca addition on the corrosion behavior of Mg–Al–Mn alloy, Appl. Surf. Sci. **369**, 92–100 (2016)
38. R.Q. Hou, C.Q. Ye, C.D. Chen, S.G. Dong, M.Q. Lv, S. Zhang, J.S. Pan, G.L. Song, C.J. Lin, Localized corrosion of binary Mg–Ca alloy in 0.9 wt% sodium chloride solution, Acta. Metall. Sin. (Engl. Lett.) **29**, 46–57 (2016)

39. R.C. Zeng, X.T. Li, S.Q. Li, F. Zhang, E.H. Han, In vitro degradation of pure Mg in response to glucose, Sci. Rep. **5**, 13026 (2015)
40. Y. Zhang, J. Li, J. Li, Effects of calcium addition on phase characteristics and corrosion behaviors of Mg-2Zn-0.2Mn-xCa in simulated body fluid, J. Alloy. Compd. **728**, 37–46 (2017)
41. W.C. Jian, W.G. Xing, H.F. Peng, M.P. Li, J.D. Wen, Effect of heat treatment on corrosion and electrochemical behaviour of Mg-3Nd–0.2Zn–0.4Zr (wt%) alloy, Electrochim. Acta **52**, 3160–3167 (2007)
42. D.J. Lin, F.Y. Hung, M.L. Yeh, H.P. Lee, T.S. Lui, Development of a novel micro-textured surface using duplex surface modification for biomedical Mg alloy applications, Mater. Lett. **206**, 9–12 (2017)
43. Z. Shi, M. Liu, A. Atrens, Measurement of the corrosion rate of magnesium alloys using Tafel extrapolation, Corros. Sci. **52**, 579–588 (2010)
44. B.S.J. Bin, Y.T. Tan, K.S. Fong, M.J. Tan, Effect of severe plastic deformation and post-annealing on the mechanical properties and bio-corrosion rate of AZ31 magnesium alloy, Procedia Eng. **207**, 1475–1480 (2017)
45. D. Song, A. Ma, J. Jiang, P. Lin, D. Yang, J. Fan, Corrosion behavior of equal-channel-angular-pressed pure magnesium in NaCl aqueous solution, Corros. Sci. **52**, 481–490 (2010)
46. N. Saikrishna, G.P.K. Reddy, B. Munirathinam, B.R. Sunil, Influence of bimodal grain size distribution on the corrosion behavior of friction stir processed biodegradable AZ31 magnesium alloy, J. Magnes. Alloy. **4**, 68–76 (2016)
47. C.L.P. Silva, A.C. Oliveira, C.G.F. Costa, R.B. Figueiredo, M.F. Leite, M.M. Pereira, V.F.C. Lins, T.G. Langdon, Effect of severe plastic deformation on the biocompatibility and corrosion rate of pure magnesium, J. Mater. Sci. **52**, 5992–6003 (2017)
48. K.D. Ralston, N. Birbilis, C.H.J. Davies, Revealing the relationship between grain size and corrosion rate of metals, Scr. Mater. **63**, 1201–1204 (2010)
49. N. Dinodi, A.N. Shetty, Electrochemical investigations on the corrosion behaviour of magnesium alloy ZE41 in a combined medium of chloride and sulphate, J. Magnes. Alloy. **1**, 201–209 (2013)
50. H. Feng, S.H. Liu, Y. Du, T. Lei, R.C. Zeng, T.C. Yuan, Effect of the second phases on the corrosion behavior of the Mg-Al-Zn alloys, J. Alloys. Comp. **695**, 2330–2338 (2017)
51. A.D. King, N. Birbilis, J.R. Scully, Accurate electrochemical measurement of magnesium corrosion rates; a combined impedance, mass-loss and hydrogen collection study, Electrochim. Acta. **121**, 394–406 (2014)
52. S.H. Mohajernia, S. Hejazi, A. Eslami, M. Saremi, Modified nanostructured hydroxyapatite coating to control the degradation of magnesium alloy AZ31 in simulated body fluid, Surf. Coat. Tech. **263**, 54–60 (2015)
53. A. Srinivasan, C. Blawert, Y. Huang, C.L. Mendis, K.U. Kainer, N. Hort, Corrosion behavior of Mg-Gd-Zn based alloys in aqueous NaCl solution, J. Magnes. Alloy. **2**, 245–256 (2014)
54. J.H. Nordlien, S. Ono, N. Masuko, K. Nisancioglu, A TEM investigation of naturally formed oxide films on pure magnesium, Corros. Sci. **39**, 1397–1414 (1997)
55. H.B. Yao, Y. Li, A.T.S. Wee, An XPS investigation of the oxidation/corrosion of melt-spun Mg, Appl. Surf. Sci. **158**, 112–119 (2000)
56. M. Santamaria, F.D. Quarto, S. Zanna, P. Marcus, Initial surface film on magnesium metal: A characterization by X-ray photoelectron spectroscopy (XPS) and photocurrent spectroscopy (PCS), Electrochim. Acta. **53**, 1314–1324 (2007)
57. M. Liu, S. Zanna, H. Ardelean, I. Frateur, P. Schmutz, G. Song, A. Atrens, P. Marcus, A first quantitative XPS study of the surface films formed, by exposure to water, on Mg and on the Mg–Al intermetallics: Al3Mg2 and Mg17Al12, Corros. Sci. **51**, 1115–1127 (2009)
58. G.L. Makar, J. Kruger, Corrosion studies of rapidly solidified magnesium alloys, J. Electrochem. Soc. **137**, 414–421 (1990)
59. S.R. Soniya, V.M. Nair, Synthesis and characterization of nanostructured Mg(OH)2 and MgO, Int. J. Sci. Res. **5**, 197–203 (2016)
60. C.R. Weber, G. Knörnschild, L.F.P. Dick, The negative-difference effect during the localized corrosion of magnesium and of the AZ91HP alloy, J. Braz. Chem. Soc. **14**, 584–593 (2013)
61. L. Yang, Y. Huang, Q. Peng, F. Feyerabend, K.U. Kainer, R. Willumeit, N. Hort, Mechanical and corrosion properties of binary Mg–Dy alloys for medical applications, Mater. Sci. Eng. C **176**, 1827–1834 (2011)
62. Z.P. Cano, M. Danaie, J.R. Kish, J.R. McDermid, G.A. Botton, G. Williams, Physical characterization of cathodically-activated corrosion filaments on magnesium alloy AZ31B, Corrosion **71**, 146–159 (2015)
63. Z.P. Cano, J.R. McDermid, J.R. Kish, Cathodic activity of corrosion filaments formed on Mg alloy AM30, J. Electrochem. Soc. **162**, 732–740 (2015)
64. P. Schmutz, V. Guillaumin, R.S. Lillard, J.A. Lillard, Influence of dichromate ions on corrosion processes on pure magnesium, J. Electrochem. Soc. **150**, B99–B110 (2003)
65. T. Al-Samman, X. Li, Sheet texture modification in magnesium-based alloys by selective rare earth alloying, Mater. Sci. Eng. A **528**, 3809–3822 (2011)
66. G.P.K. Reddy, B.R. Sunil, B. Balakrishna, Joining of AZ31 Mg alloy sheets by friction stir welding and investigating corrosion initiated failure, Materials Today: Proceedings **4**, 6712–6717 (2017)
67. N. Li, Y. Zheng, Novel magnesium alloys developed for biomedical application: a review, J. Mater. Sci. Technol. **29**, 489–502 (2013)
68. E.L. Zhang, D.S. Yin, L.P. Xu, L. Yang, K. Yang, Microstructure, mechanical and corrosion properties and biocompatibility of Mg–Zn–Mn alloys for biomedical application, Mater. Sci. Eng. C **29**, 987–993 (2009)


**Cite this article as**: Abdelkader Hanna, Achour Dakhouche, Kamel Tirsatine, Ali Sari, Yazid Khereddine, Djamel Bradai, Hiba Azzeddine, Effect of hot rolling on the corrosion behavior of AZ31 magnesium alloy, Metall. Res. Technol. **116**, 109 (2019)